Steel and Composite Structures, *Vol. 20, No. 6 (2016) 1221-1236*
DOI: http://dx.doi.org/10.12989/scs.2016.20.6.1221

Cyclic and static behaviors of CFT modular bridge pier with enhanced bracings

Dongwook Kim *, Chiho Jeon [a] and Changsu Shim [b]

Department of Civil Engineering, Chung Ang University, Seoul, Republic of Korea

(*Received November 11, 2015, Revised January 20, 2016, Accepted February 11, 2016*)

Abstract. Modular structures consist of standardized modules and their connections. A modular bridge pier is proposed to accelerate bridge construction. Multiple concrete-filled steel tubes (CFTs) using commercial steel tubes were chosen as the main members. Buckling restrained bracings and enhanced connection details were designed to prevent premature low-cycle fatigue failure upon cyclic loading. The pier had a height of 7.95 m, widths of 2.5 m and 2.0 m along the strong and weak axis, respectively. Cyclic tests were performed on the modular pier to investigate structural performance. Test results showed that four CFT columns reached yielding without a premature failure of the bracing connections. The ultimate capacity of the modular pier was reasonably estimated based on the plastic-hinge-analysis concept. The modular CFT pier with enhanced bracing showed improved displacement ductility without premature failure at the welding joints.

Keywords: modular bridge pier; CFT; buckling restrained bracing; cyclic test; ductility

1. Introduction

There are driving forces that impose the use of prefabrication techniques in the construction industry to lower costs, the need to achieve a competitive edge, the lack of skilled construction labor, and the need to increase productivity (FMI corporation 2013). According to McGraw Hill's survey, nearly all participants (98%) are expected to be involved with some prefabrication/ modularization on some of their projects (McGraw Hill Construction 2011). The modular concept utilizes commercial products to minimize fabrication effort and to accommodate a certain range of design parameters. Typical bridge structures are the most appropriate for modularization of their components. The connection details and their structural performance are essential considerations in design.

There were many experimental studies to accelerate construction of bridge substructures. Shim *et al*. (2008a) examined precast piers with bonded prestressing bars and steel tubes. All of the specimens exhibited a flexural failure mode in the plastic hinge region. A higher steel ratio elicited benefits after reaching the maximum load capacity of the columns. Shim *et al*. (2008b) stated that composite columns showed better seismic performance in terms of the ductility and energy

*Corresponding author, Ph.D. Candidate, E-mail: clearup7@cau.ac.kr
[a] Master Student, E-mail: chihobeer@cau.ac.kr
[b] Professor, E-mail: csshim@cau.ac.kr

http://www.techno-press.org/?journal=scs&subpage=6 ISSN: 1229-9367 (Print), 1598-6233 (Online)

absorption capacity compared to reinforced concrete columns with similar steel ratios. Their research on prefabricated circular composite columns with a low steel ratio showed a significant increase in the maximum column strength as the applied prestressing force increased (Shim *et al*. 2011). Chou et al. showed that segmental precast unbounded posttensioning bridge columns can safely resist lateral cyclic forces and undergo large nonlinear displacements without experiencing significant or sudden loss of strength (Chou and Chen 2006). Elgawady *et al*. (2012) showed that the analysis of segmental piers that consisted of concrete filled fiber reinforced plastics (FRP) tubes yielded a significant confinement effect on the performance of the investigated piers. However, it is difficult for these prefabricated columns to be standardized as modules.

Concrete filled steel tubes (CFTs) using commercial products were suggested as column modules owing to their excellent structural performance, light weight, transparency and ease of erection and connection (Shim *et al*. 2014). Fig. 1 shows the design concept of the modular bridge pier. Despite the numerous merits of the modular bridge pier system, the application of the CFT modular pier is limited by many variables that need to be resolved, such as strength, stiffness, connection details, and seismic design. As a preliminary experiment of the modular bridge pier, a bridge pier was fabricated in accordance to the suggested fabrication method with a diameter of 165.2 mm and a thickness of 6.0 mm (Ma *et al*. 2012). The height of the pier was 3.0 m, and the longitudinal and transverse spacing of the columns were 1.0 m and 0.8 m, respectively. From the test results, the cracks at the welding toe of the upper bracings were occurred before the CFT columns reached yielding. Even though there was section loss of the steel tubes, four columns showed yielding. Premature failure of the connections should be prevented to improve the seismic performance of the modular pier. In order to prevent the premature failure, the failure at the column should not be damaged by bracing before the column elicits the full flexural capacity.

Among the seismic performance upgrading systems, there are several options that are normally

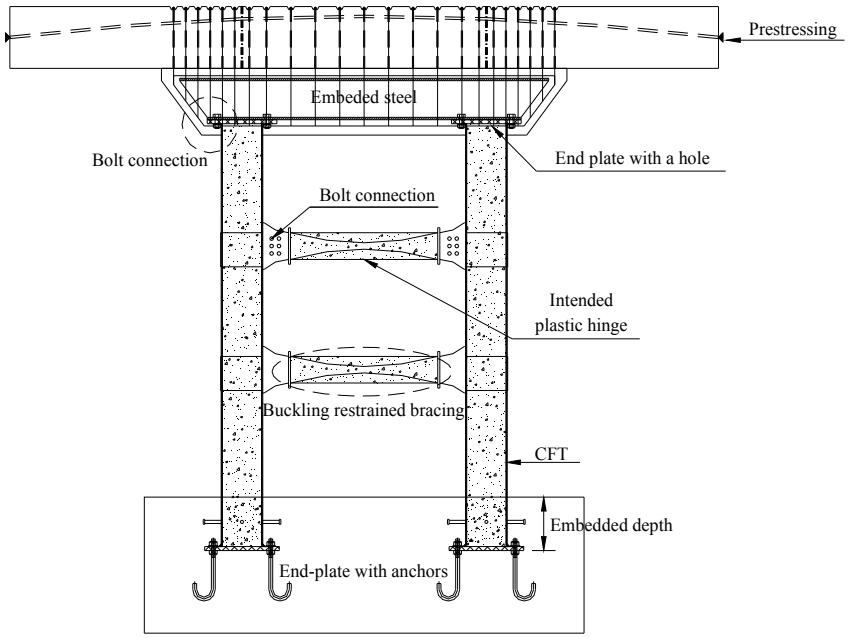

Fig. 1 Modular pier cap

available, one of which is to employ energy dissipation devices, such as friction, viscoelastic and metallic dampers, buckling-restrained braces (BRBs), and others. The energy input owing to a strong earthquake is expected to be greatly dissipated by these devices. Therefore, of these devices are damaged, they make the rehabilitation easy after the earthquake, since they are designed to be replaceable.

A buckling restrained bracing, which is a type of a concentrically braced frame, is particularly configured to yield a full hysteresis loop to absorb effectively the vibrational energy generated by the earthquake. This minimizes the damage to the framework resulting from the shock of the earthquake. Kim et al. stated that equivalent damping ratios of SDOF structures with buckling restrained bracing (BRBs) generally increase as the stiffness of BRBs increase (Kim and Choi 2003).

In this paper, a new modular bridge column system was proposed to prevent the connection failure through an experiment on the modular bridge pier with BRBs, conducted on a full-scale test specimen that was, 7.95 m height. The work presented in this paper attempts to improve the cyclic performance by investigating the inelastic hysteresis, behavior of the newly proposed, plastic-hinge-analysis concept. The proposed plastic-hinge-analysis concept is expected to provide a way of assessing seismic performance.

2. Experimental program

2.1 Test specimen

A test specimen was designed to investigate the structural performance based on static and cyclic loading conditions. Four circular CFTs were connected by different lengths of BRBs. At the joints between circular CFT columns and bracings, steel plates were connected by fillet welding. The circular CFT columns were embedded into the concrete footing. For the design of the connection under seismic actions, both the Association of State Highway and Transportation Officials (AASHTO) and the American Concrete Institute (ACI) codes specify development lengths for bars embedded in concrete (ACI 2014 and AASHTO 2010).

Local stability is controlled by limiting the dimension/thickness (*D/t*) ratio, as shown in Table 1. The stability limits of the codes take different forms, and they result in different limits. This is because the limiting *D/t* ratios for using the plastic capacity of circular CFT with a steel yield stress of 315 MPa are approximately 73.3, 73.0, 73.0 and 67.1 for the LRFD, AISC, ACI and Eurocode-4 provisions, respectively (AISC 2005, ACI Committee 318 2014, AASHTO LRFD 2010 and Eurocode 4 2004) . Four circular CFT columns were installed with an outer diameter 508.2 mm and were proportional to a *D/t* ratio equal to 17, in accordance to the design provisions in order to constrain local stability. Each column was connected with buckling restrained bracing with a 16 mm thickness plate.

Table 1 D/t ratio of CFT member

Design code	D/t ratio limit	
	Limit	Calculation
LRFD	$0.11E/f_y$	73.3
ACI-318 AISC-LRFD	$\sqrt{8}E_s/f_y$	73.0
Eurocode-4	$90(235/f_y)$	67.1

Fig. 2 shows the modular CFT column test specimen having a height of 7,950 mm (including the footing and the pier cap). The measured length of the column from the top of the foundation (5,800 mm) to the level of the lateral loading aspect ratio of the single CFT column was equal to 11. The column specimen consisted of three layers of six bracings and a pier cap module. The column module was 5,830 mm tall including a column that was embedded into the footing. The pier cap was a rectangular concrete block and its dimensions were 5,500 mm × 3,000 mm × 1,900 mm.

The deadweight of the bridge superstructures needed to be transmitted from the pier cap to the columns. In order to solve this problem, a steel-embedded-composite pier table was proposed. The steel columns were connected to the embedded steel member using bolt connections. The embedded steel sections were 4,400 mm (length) × 407 mm (width) × 428 mm (height) and the thickness of flanges and the web were 35 mm, and 20 mm, respectively. The pier table was then connected to precast the pier cap segments using vertical reinforcements. After assembly, the pier cap segments were connected using transverse prestressing. Epoxy bonding was provided for all connected surfaces. The CFT columns were embedded into the footing a depth equal to 1.5 times (770 mm) the depth of the CFT diameter using eight welded studs. Longitudinal and transverse spacing of the columns were 2.5 m and 2.0 m, respectively. Three layers of six bracings were installed using bolt connection.

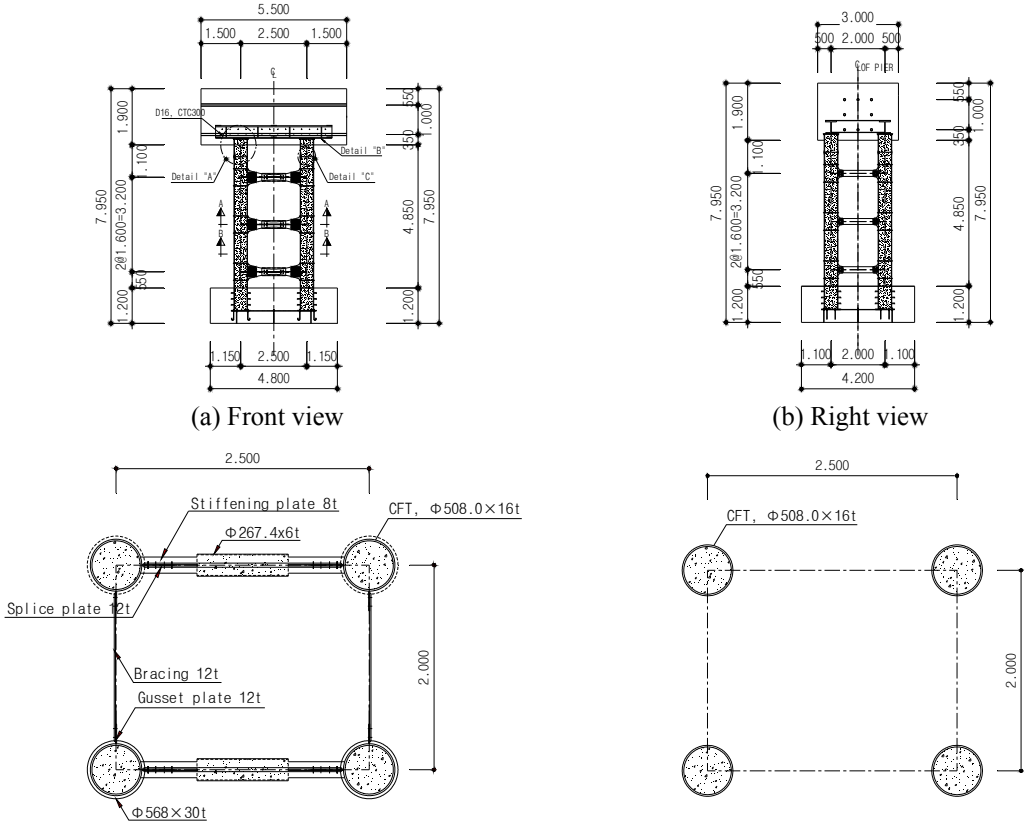

Fig. 2 Test specimen

2.2 Test specimen

The designed and measured (on the day of the experiment) compressive strengths of the concrete used were 40 MPa and 42 MPa, respectively. Structural steel tubes of the circular CFT columns and bracings had yield and tensile strengths of 315 MPa and 490 MPa, respectively.

The construction phases are as shown in Fig. 3. The footing and column modules were fabricated. The column modules had concrete inside before they were assembled, as shown in Fig. 3(a). Steel tubes for BRB members were also filled with concrete, as shown in Fig. 3(e). After installing the column module into the footing module, concrete was poured up to the top of the footing level. Then the pier cap module and bracing modules were then assembled using welding and bolting connection, respectively.

The BRB technology is currently undergoing development, with a growing number of structures using BRBs as the primary lateral force-resisting system (D'Aniello 2007). The bracings consist of a ductile, dog-bone shaped steel core (rectangular plate rods) having a thickness of 16 mm in a continuous concrete filled tube (Φ 267.4 × 6 t), as shown in Fig. 4. This bracing features a steel core encased in a concrete-filled steel hollow tube. The flat 16 mm spliced plate and the 16 mm gusset plate were bolted with a dog-bone-shaped flat bracing. These bracings were expected to alleviate the stress concentration near the connections, and prevent premature failure of the steel tubes by cyclic loads.

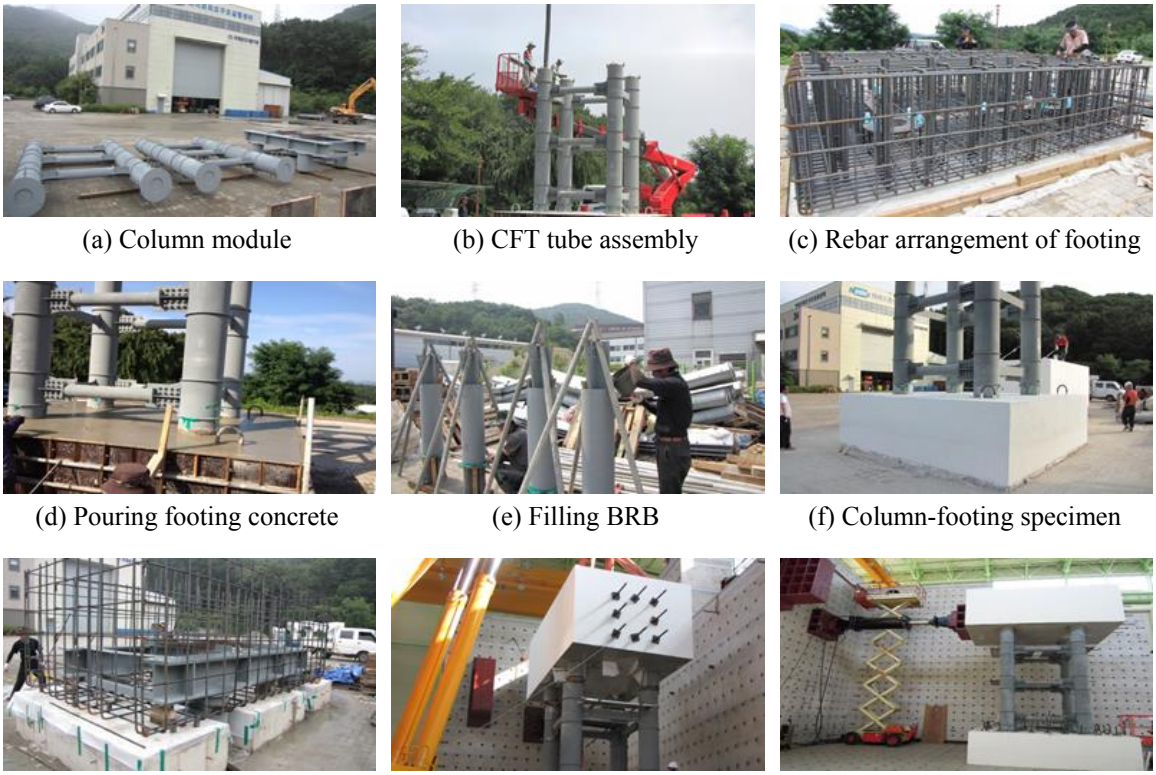

(a) Column module (b) CFT tube assembly (c) Rebar arrangement of footing

(d) Pouring footing concrete (e) Filling BRB (f) Column-footing specimen

(g) Pier cap (h) Pier cap-column assembly (i) Completed specimen

Fig. 3 Fabrication procedure

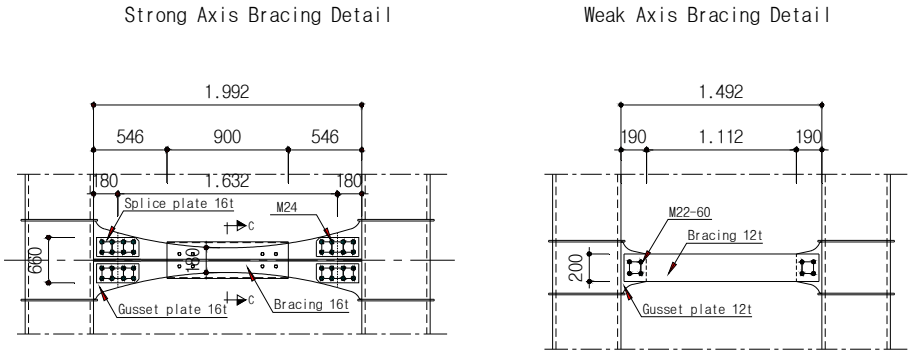

Fig. 4 Bracing details

2.3 Measurement plan

The behavior of the modular CFT pier structure was observed by measuring the strain of the CFT columns, bracing connections and plastic hinge location as shown in Fig. 5. The global behavior was estimated by measuring the lateral displacements using displacement transducers (LVDT). Three LVDTs were positioned at all bracing levels to investigate the displacement owing to the lateral load along the strong axis, as shown in Fig. 5(a). Multiple strain gauges were also attached around the steel tubes at each level of S1, S2, S3, S4 and S5 to investigate the behavior of circular CFT columns when a lateral load was applied as illustrated in Figs. 5(c) and (d). Plastic strain gauges at the intentional plastic region of bracing were attached to investigate the behavior of the bracing as shown in Fig. 5(e). The movement of the footing by lateral loading was also checked using displacement transducers. A data acquisition system was used to record the applied load and the readings of the sensors at regular intervals during the tests.

2.4 Cyclic tests

The cyclic test of the modular CFT column with BRBs was conducted, as shown in Fig. 6. An actuator with a 3,000 kN load capacity was used to apply the lateral load at the highest level of the specimen. At the first stage, a cyclic load was introduced at the strong axis using a displacement control method with a maximum load of 1,798 kN. The actuator provides a maximum allowable stroke of 1,500 mm for the cyclic loading condition. Bridge piers are normally designed to withstand approximately 10% of their compressive strength. However, with the limits of the setup system, 1.8% of the compressive axial force was applied by the dead weight of the pier cap module.

The lateral cyclic load was applied to the center of the pier cap, as shown in Fig. 6. In order to determine the applied displacement, the expected yield displacement and yield strain were calculated. Cyclic loads were applied in thirty six repeated cycles in order to attain the lateral displacement of the column. The maximum value of the displacement was 48.63 mm, equal to 1.03% of the lateral drift ratio. During the period spanning cycles 1-12, the drift ratio was increased with a speed of 1.8 mm/min. speed, corresponding to a drift ratio in the range of 0.03-0.16%. During the period spanning cycles 13-26, the drift ratio was increased with a speed of 3.6 mm/min., corresponding to drift ratio in the range of 0.21-0.52%. For the period spanning cycles 27- 30, the drift ratio speed was increased to 7.2 mm/min., corresponding to drift ratio in the range

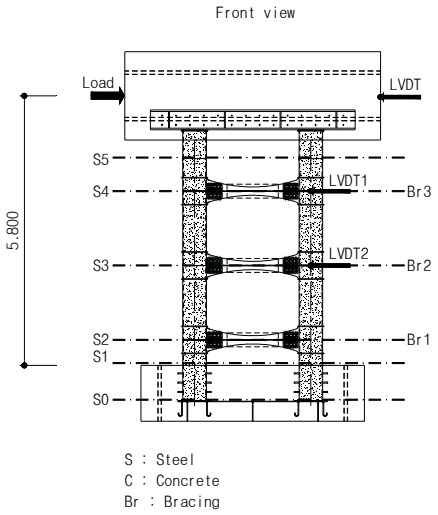

(a) Front view

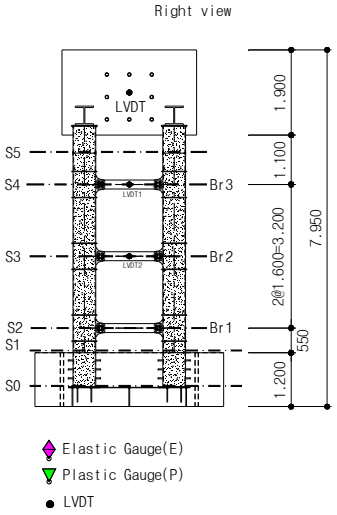

(b) Right view

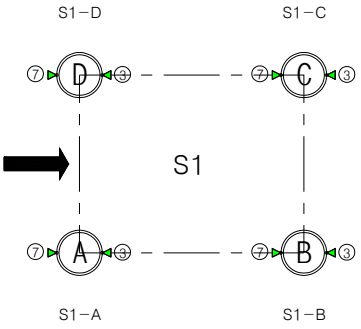

(c) S1 level

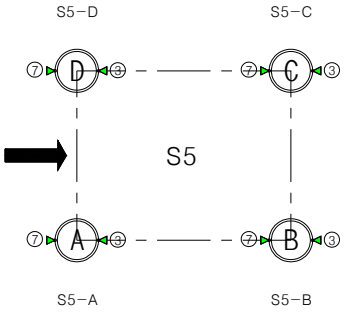

(d) S5 level

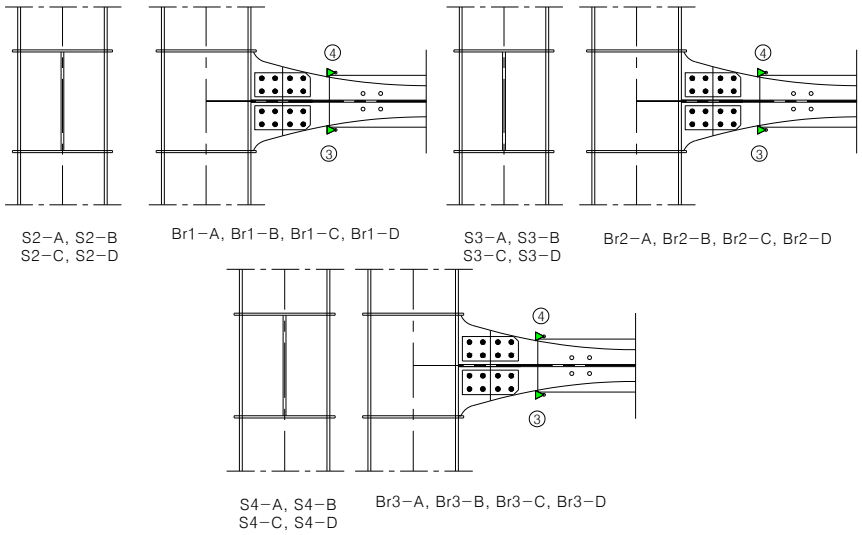

(e) Gauge plan of bracing

Fig. 5 Measurement plan

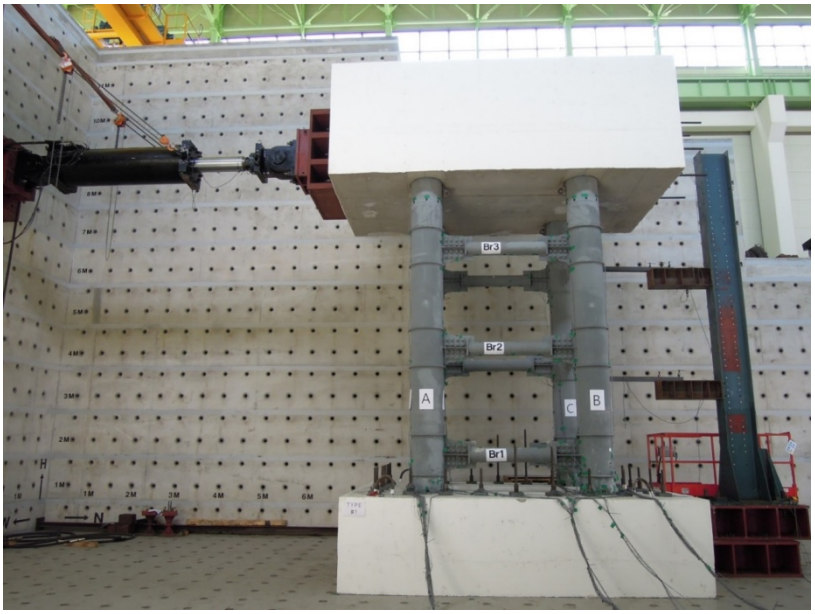

Fig. 6 Test setup

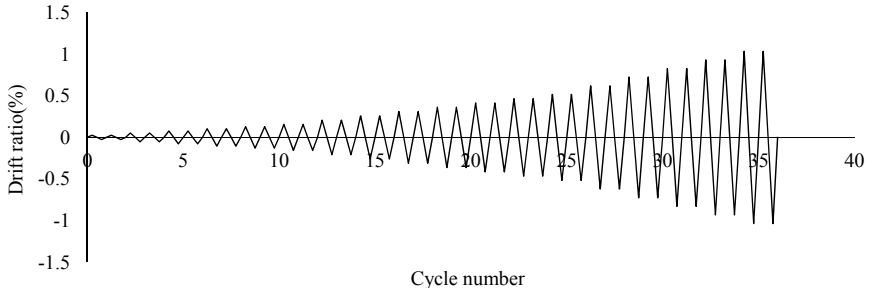

Fig. 7 Loading pattern according to drift ratio

of 0.62- 0.72%. Finally, during the period spanning cycles 31-36, the cyclic load was applied with a speed of 57.6 mm/min.

At the second stage, the static load was introduced at the strong axis by using the displacement control method with a maximum load of 2,587 kN. The static load was applied at a speed of 10 mm/min. The maximum value of the elicited displacement was 134.04 mm, which corresponded to a drift ratio of 2.84%.

3. Test results

3.1 Cyclic behavior

Figs. 8 and 9 show the load displacement curve and the envelope curve of the test specimen, respectively. The peak lateral forces at a drift ratio of 1.03% are 1,798 kN and 1,814 kN for the positive and negative directions, respectively. The maximum displacements at a drift ratio of 1.03%

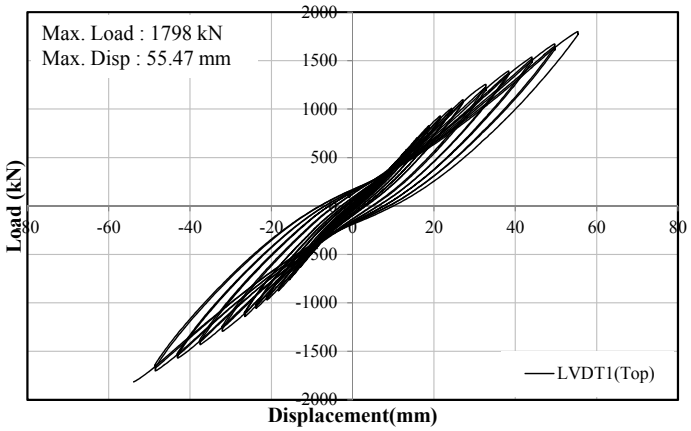

Fig. 8 Load-displacement hysteresis curves

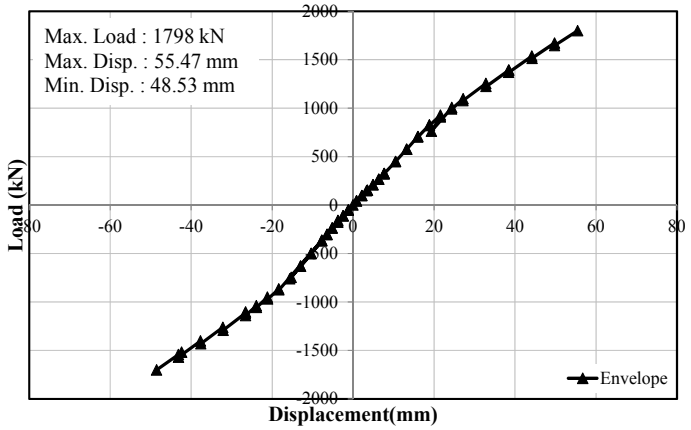

Fig. 9 Load-displacement envelope curve

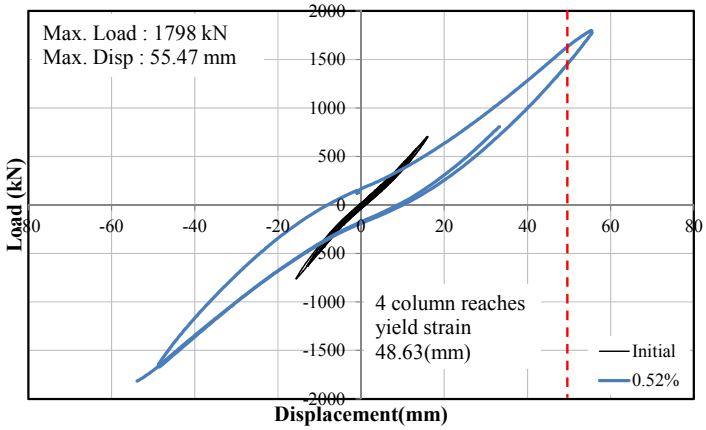

Fig. 10 Load-displacement of initial and final loading stage

were 55.47 mm and 53.86 mm for the positive and negative directions, respectively. Connections with the footing and the pier cap modules did not show any significant damages as a result of the cyclic loading. Premature failure at the joints was not observed with load up to maximum load.

The test specimens behaved in a ductile manner with the formation of plastic hinges at the end of the CFT columns. It was found that the specimen showed an essentially linear behavior at the early stage of its loading. Local yielding started to develop at the end of the CFT column at a rotation of 0.52% that can be verified by the changes in the strain values of both strain gauges. On the other hand, no obvious deformation was observed in the concrete. This phenomenon can be regarded as an evidence of the yielding of the CFT column.

The energy dissipation capacity of connections is one of the most important factors in their seismic performance. The dissipated energy is defined to be the area of the hysteresis loop formed by the relationship of moment and rotation. The energy dissipation capacity of the specimens stably increased with the increase in the load amplitude of the hysteresis loops up to the maximum

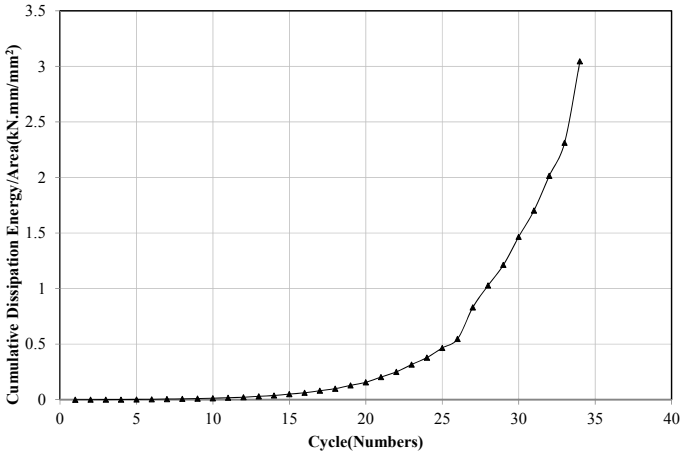

Fig. 11 Energy dissipation curve

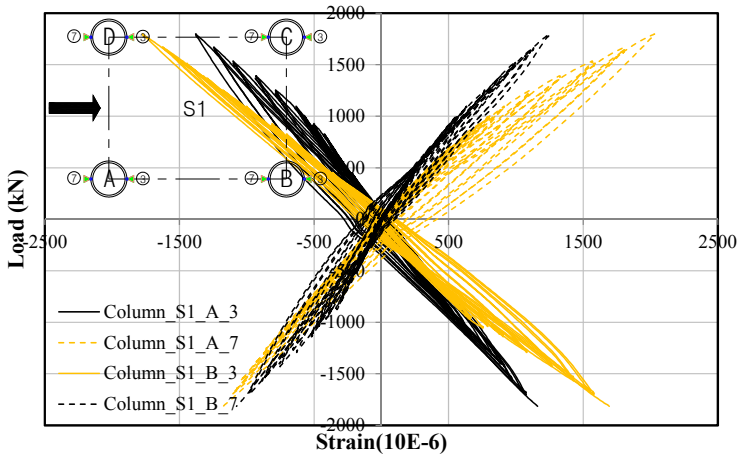

Fig. 12 Load-strain curves of CFT column (S1 level)

load. The hysteretic energy dissipation of the specimens was evaluated based on the cumulative dissipation energy as shown in Fig. 11. It was found that the hysteretic energy dissipation increased as the column drift increased. After the CFT column yielding (26 cycles, drift ratio 0.52%), the hysteretic energy was enhanced by 5.5 times at the final stage compared to the initial stages of the loading protocol.

Fig. 12 shows the load strain curves of the bottom of CFT column. Plastic strain was observed at the bottom part of the CFT column. The yield strain of the CFT column is expected to be 1,500 $\mu\varepsilon$. The yield load was defined as the strain of the four CFT columns that reached the yield strain. When the strain of the column reached the yield strain, a higher strain was exhibited than the strain of the bracing connection. At the final stage of the loading protocol, the strain of the bracing connection was in the elastic range.

3.2 Static behavior

Seismic performance of bridge piers can be evaluated by displacement ductility. Yield displacement has been distinctly defined by many researchers worldwide. In general, the definition of the yield displacement is determined on the basis of the strain of steel in the plastic-hinge region once it reached its yielding point (Roeder *et al*. 2009).

The modular pier maintained the load with excellent ductility up to the maximum load, as shown in Fig. 13. The displacement ductility was evaluated for the positive direction at the second stage of the loading pattern. The yield load (1,843 kN), defined by the yield strain, and the yield displacement (48.63 mm) are shown in Fig. 13. After the cyclic loading tests, conducted at drift ratios up to 1.03%, a static load was applied to the test specimen to evaluate the ultimate strength and its ductility. The yielding behavior started to develop at a drift ratio of approximately 0.52% for the cyclic loading of the first stage of the loading pattern. The ductility ratio at the end of the test was higher than 2.76 for the static loading. Owing to the stroke limitation of the actuator, the exact displacement ductility could not be calculated. Judging from the observations, the improved details of bracings and connections contributed to the ductile behavior without any premature failure of the column face at the connections comparing to the previous test specimen. The ductility ratio of the specimen is defined as the ratio of the ultimate displacement to the yield

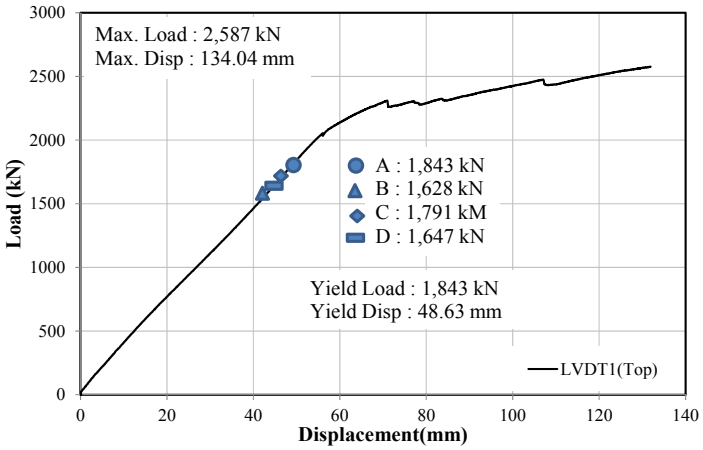

Fig. 13 Load-displacement curve of static loading

displacement. In previous research (Shim *et al*. 2014 and Ma *et al*. 2012), the displacement ductility was 2.52. However, in this research, the displacement ductility was higher than 2.76 with maintenance of its strength. Owing to the limit of the actuator's stroke, the exact displacement ductility could not be obtained.

In order to evaluate the onset of yielding of the CFT columns at the bottom and the top parts, measured strain values are plotted in Fig. 14. The maximum value of the load and displacement were 2,587 kN and 134.04 mm, respectively. The strain at the top of the columns based on the extrapolation of the measured value at the S5 level showed yield strain. The bottom part of the column at the S1 level also indicated plastic behavior. As listed in Table 1, four circular CFT columns were installed with an outer diameter of 508.2 mm, being proportional to a *D/t* ratio equal to 17, in accordance to the design provisions and in order to constrain local stability. Local buckling was not observed at any surface of the four CFT columns for applied loads up to the maximum load.

The plastic stress-block concept is extensively used to calculate the strength of the CFT section. However, it is difficult to evaluate the flexural strength of multiple CFT columns with bracings

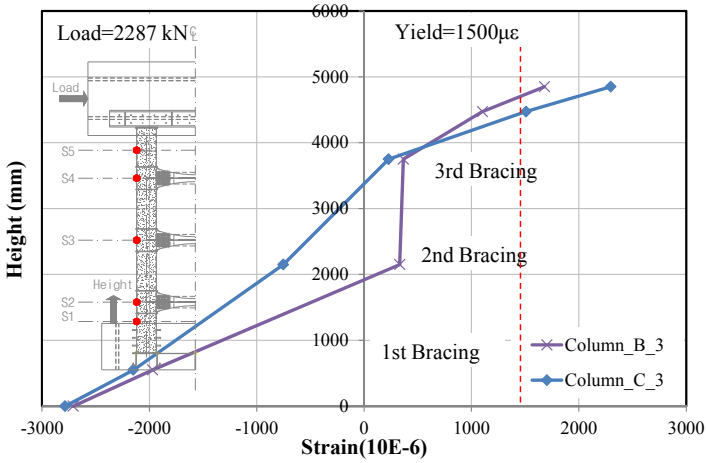

Fig. 14 Load-strain curves of CFT column according to height

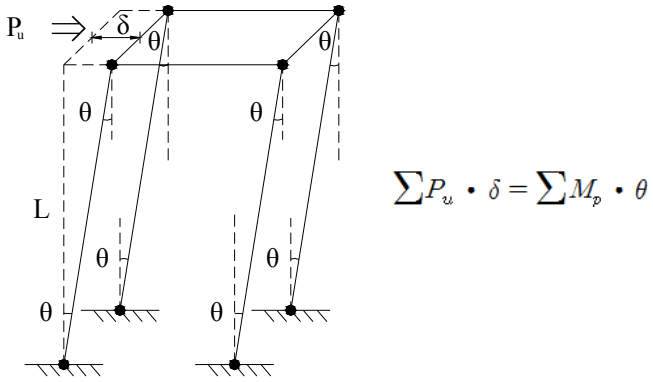

$$\sum P_u \cdot \delta = \sum M_p \cdot \theta$$

Fig. 15 Plastic hinge analysis model

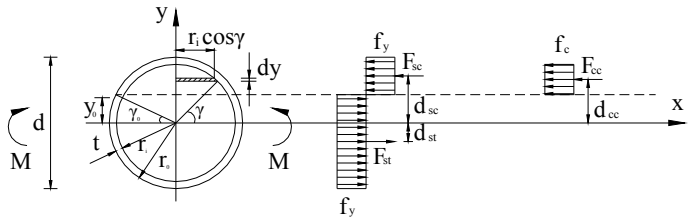

Fig. 16 Plastic stress distribution

Table 2 Plastic hinge analysis results

Full scale test specimen		Experiment/Calculation
Maximum load (Experiment)	2,587.0 kN (134.04 mm)	1.18
Plastic load (Calculation)	2,179.3 kN	

using the plastic stress-block concept since it is difficult to define a plastic neutral axis. Thus, a plastic-hinge analysis method was adopted to evaluate the flexural strength of the pier, as shown in Fig. 15. Table 2 summarizes the plastic-hinge analysis results and experimental results. The plastic load was calculated to be 2,179 kN and the ultimate load in the experiment was 2,587 kN. The experimental result was 1.18 times higher than that of the calculation. Fig. 16 represents the stress distribution of the CFT section for the calculation of the plastic moment capacity, M_p. Thus, the plastic-hinge analysis concept can be used for the evaluation of the ultimate strength of multi modular CFT columns.

3.3 Local behavior

The strain distribution of the CFT column is an important factor for the evaluation of its structural performance. Fig. 17 represents the strain distribution of two columns at the S1 level. Each column showed tensile and compressive strain at the plastic hinge region. As assumed in the calculation of the plastic moment capacity of the CFT columns, the measured strain values indicated that yielding of the full section occurred at the maximum load.

In order to evaluate the structural performance of the CFT column, the interaction between the steel and the concrete parts is very important. The bond capacity is interrelated with the slip at the steel-concrete interface. Fig. 18 shows the cutting section of the CFT column (S1 level) after the test. The separation between the steel tube and the concrete core was not observed. There was no local buckling at any surface of the steel tube.

At the final stage of the loading protocol, the bracing showed bending behavior. Fig. 19 shows the stress-strain curves of the bracing at BR2. As the lateral load increased, the strain of the bracing was not increased after CFT columns reached the yield point. From this observation, the minimum section area of the bracings can be derived. In terms of the bracing design, Watanabe *et al*. (1998) showed the effectiveness of the BRB and investigated the effect of the outer tube configuration on the overall load capacity of the brace. As they discussed in their research results, the stiffness of the bracing can be a useful design parameter for seismic design.

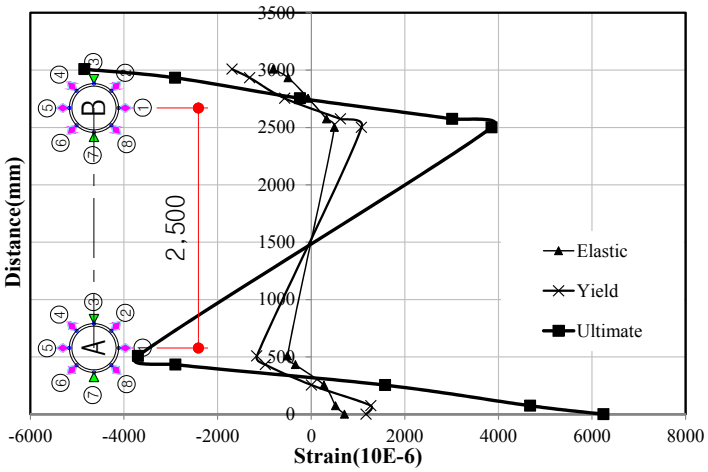

Fig. 17 Strain distribution of CFT columns at S1 level

(a) (b)

Fig. 18 Cutting section of CFT column (after test)

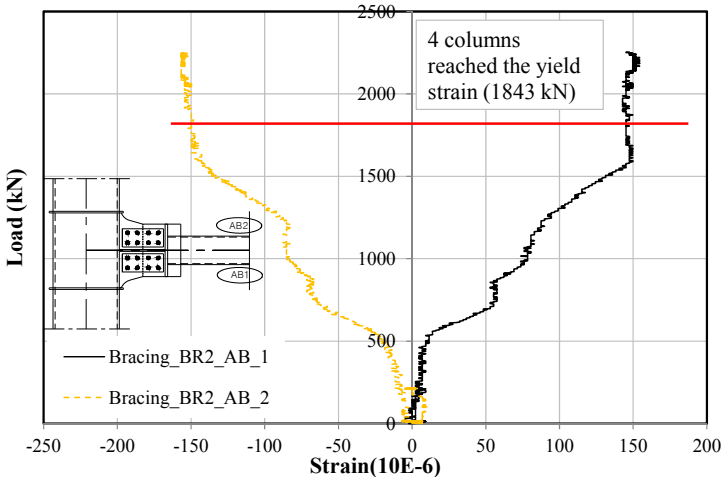

Fig. 19 Load-strain curves of a bracing

4. Conclusions

In this paper, a new modular bridge column system is proposed by investigating the inelastic hysteretic behavior of a real sized specimen. Through the quasi-static test, the enhanced details of the bridge pier were verified and essential design considerations were derived. Based on the test results, the following conclusions are derived:

(1) The proposed details of bracings and their connection showed improved structural performance in terms of the full plastic behavior of the columns than the previous research. The displacement ductility of modular CFT column with BRB specimen was higher than 2.76 without premature failure at the joints.
(2) The energy dissipation capacity of the specimens showed a stable increase with increases in the load amplitude of the hysteresis loops up to the maximum load. In order to enhance the energy dissipation capacity, the bracing needs to deliver the load properly. Therefore, the premature failure at the bracing joints should be prevented until the CFT columns reach the yield.
(3) A simplified design method for the ultimate strength of multiple CFT columns was suggested based on the plastic-hinge analysis concept. The plastic-hinge analysis method provided a simple and reliable evaluation method for the prediction of the resistance of multiple CFT columns. The plastic hinge analysis results were compared with test results and yielded conservative estimations with a difference of 18%.
(4) The BRB improved the overall behavior of the modular pier. The measured response of the bracings showed that the section dimensions can be reduced to provide the full plastic capacity of each CFT column. The optimum design of the bracings needs further investigation.

Acknowledgments

This research was supported by the Chung-Ang University Excellent Student Scholarship in 2015 and a grant from the Construction Technology Innovation Program (10CTIPB01-Modular Bridge Research and Business Development Consortium) funded by Ministry of Land, Transportation and Maritime Affairs(MLTM) of the Korean Government.

References

AASHTO (2010), LRFD Bridge Design Specifications, (3rd Ed.), American Association of State Highway and Transportation Officials, Washington, D.C., USA

ACI Committee 318 (2014), Building Code Requirements for Structural Concrete (ACI318-11) and Commentary, American Concrete Institute.

ACI Committee 408 (2001), Splice and Development Length of High Relative Rib Area Reinforcing Bars in Tension (408.3-01) and Commentary (408.3R-01), American Concrete Institute, Farmington Hills, MI, USA.

AISC (2005), Specification for Structural Steel Buildings, ANSI/AISC 360-05, American Institute of Steel Construction, Inc., Chicago, IL, USA.

American Association of State Highway and Transportation Officials (2010), AASHTO LRFD Bridge Design Specification, (5th Edition).

Chou, C.C. and Chen, Y.C. (2006), "Cyclic tests of post-tensioned precast CFT segmental bridge columns with unbounded strands", *Earthq. Eng. Struct. Dyn.,* **35**(2), 159-175.
D'Aniello, M. (2007), "Steel dissipative bracing systems for seismic retrofitting of existing structures: Theory and testing", Ph.D. Thesis; University of Naples "Federico", Naples, Italy.
Elgawady, M.A. and Dawood, H.M. (2012), "Analysis of segmental piers consisted of concrete filled FRP tubes", *Eng. Struct.,* **38**, 142-152.
Ellobody, E., Young, B. and Lam, D. (2006), "Behaviour of normal and high strength concrete-filled compact steel tube circular stub columns", *J. Construct. Steel Res.*, **62**(7), 706-715.
Eurocode 4 (2004), Design of Composite Steel and Concrete Structures - Part 1-1: General Rules and Rules for Buildings, EN1994-1, Brussels, Belgium.
FMI Corporation (2013), Prefabrication and Modularization in Construction.
Gu, Q., Zona, A., Peng, Y. and Dall'Asta, A. (2014), "Effect of buckling-restrained brace model parameters on seismic structural response", *J. Construct. Steel Res.*, **98**, 100-113.
Hassan, M.M., Ramadan, H.M., Abdel-Mooty, M.N. and Mourad, S.A. (2014), "Behavior of concentrically loaded CFT braces connections", *J. Adv. Res.,* **5**(2), 243-252.
Hu, H.T., Su, F.C. and Elchalakani, M. (2010), "Finite element analysis of CFT columns subjected to pure bending moment", *Steel Compos. Struct., Int. J.,* **10**(5), 415-428.
Kim, J. and Choi, H. (2003), "Behavior and design of structures with buckling-restrained braces", *Eng. Struct.,* **26**(6), 693-706.
Ma, H.W., Oh, H.C., Kim, D.W., Kong, D. and Shim, C.S. (2012), "Evaluation of Flexural Behavior of a Modular Pier with Circular CFT", *J. Korean Soc. Steel Construct.,* **24**(6), 725-734. [In Korean]
MagarPatil, H.R. and Jangid, R.S. (2015), "Development and analysis of passive hybrid energy dissipation system for steel moment resisting frame", *Int. J. Civil Struct. Eng.,* **5**(4), 339-352.
McGraw Hill Construction (2011), Prefabrication and Modularization: Increasing Productivity in the Construction Industry.
Roeder, C.W., Lehman, D.E. and Thody, R. (2009), "Composite action in CFT components and connections", *Eng. J.*, *AISC*, **47**(4), 229-242.
Shim, C.S., Chung, C.H. and Kim, H.H. (2008a), "Experimental evaluation of seismic performance of precast segmental bridge piers with a circular solid section", *Eng. Struct.,* **30**(12), 3782-3792.
Shim, C.S., Chung, Y.S. and Han, J.H. (2008b), "Cyclic response of concrete-encased composite columns with low steel ratio", *Struct. Build.,* **161**(2), 77-89.
Shim, C.S., Chung, Y.S. and Yoon, J.Y. (2011), "Cyclic behavior of prefabricated circular composite columns with low steel ratio", *Eng. Struct.,* **33**(9), 2525-2534.
Shim, C., Kim, D., Jung, D., Kim, I. and Chung, C. (2014), "Cyclic tests of modular CFT bridge piers", *Proceedings of 10th U.S. National Conference on Earthquake Engineering Frontiers of Earthquake Engineering*, Anchorage, AK, USA, July, pp. 1-10.
Stefan, W. (2012), "Behaviour and design of generic buckling restrained brace systems", M.S. Thesis; Department of Civil and Environmental Engineering, The University of Auckland, Auckland, New Zealand.
Watanabe, A., Hitomoi, Y., Saeki, E., Wada, A. and Fujimoto, M. (1988), "Properties of braces encased in buckling–restraining concrete and steel tube", *Proceedings of the 10th World Conference on Earthquake Engineering,* Tokyo–Kyoto, Japan, August.

CC